MiReCOL Mitigation and Remediation of CO_2 Leakage

Project no.:
608608

Project acronym:
MiReCOL

Project title:
Mitigation and remediation of leakage from geological storage

Collaborative Project

Start date of project: 2014-03-01
Duration: 3 years

D6.4

Remediation Techniques Based on Foam Injection

Status: definitive

Organisation name of lead contractor for this deliverable:
IFPEN

Project co-funded by the European Commission within the Seventh Framework Programme		
Dissemination Level		
PU	Public	X
PP	Restricted to other programme participants (including the Commission Services)	
RE	Restricted to a group specified by the consortium (including the Commission Services)	
CO	Confidential , only for members of the consortium (including the Commission Services)	

Deliverable number:	**Error! Reference source not found.**
Deliverable name:	Publication: remediation techniques based on foam injection
Work package:	WP6.4 Foam Generation Methods
Lead contractor:	IFPEN

Status of deliverable		
Action	**By**	**Date**
Submitted (Author(s))	Guillaume Batôt, Chris Hewson, Lahcen Nabzar and Marc Fleury	03/02/2017
Verified (WP-leader)	Marc Fleury	03/02/2017
Approved (SP-leader)	Marc Fleury	03/02/2017
Approved (Coordinator)	Holger Cremer	06/02/2017

Author(s)		
Name	**Organisation**	**E-mail**
Guillaume Batôt	IFPEN	guillaume.batot@ifpen.fr
Marc Fleury	IFPEN	marc.fleury@ifpen.fr
Chris Hewson	TNO	Chris.hewson@tno.nl
Lahcen Nabzar	IFPEN	lahcen.nabzar@ifpen.fr

Public abstract

This report is part of the research project MiReCOL (Mitigation and Remediation of CO_2 leakage) funded by the EU FP7 programme. Research activities aim at developing a handbook of corrective measures that can be considered in the event of undesired migration of CO_2 in the deep subsurface reservoirs. MiReCOL results support CO_2 storage project operators in assessing the value of specific corrective measures if the CO_2 in the storage reservoir does not behave as expected. MiReCOL focuses on corrective measures that can be taken while the CO_2 is in the deep subsurface. The general scenarios considered in MiReCOL are 1) loss of conformance in the reservoir (undesired migration of CO_2 within the reservoir), 2) natural barrier breach (CO_2 migration through faults or fractures), and 3) well barrier breach (CO_2 migration along the well bore).

We studied in the laboratory the capacity of foams to reduce gas flow for CO_2-brine systems in rock core sample with common surfactants, as a function of interstitial velocity and gas to water fraction. All experiments were carried out in similar Clashach sandstones with permeability between 220 and 1500 mD, and porosity in the range 10-20%. The gas and the surfactant-brine solution were co-injected at the core inlet face with a gas fraction around 0.7. We vary the interstitial velocity within two decades from about 3 ft/day up to 100 ft/day.

The performance of the generated foams was evaluated from the relative foam viscosity, the ratio of the measured pressure drop in the presence of foam to the pressure drop in single phase condition for the same interstitial velocity. Whatever the pressure and permeability/porosity, the relative foam viscosity can be described as a power law vs. the shear rate evaluated from the interstitial velocity, permeability and porosity. The exponent is close to -1 describing the shear-thinning behavior.

Based on this experimental correlation the technical feasibility of foam injection, as a mitigation

method, was numerically explored from reservoir simulations. The scenario studied is the case of a leak through a fracture in the caprock. The foam is injected at the top of the reservoir below the caprock. We show that foams can effectively reduce the leak provided the well is not too far from the leak, typically of the order of 50-10 m. The advantages and drawbacks of this remediation method are discussed.
This work was partially presented during the Society of core Analysts meeting in Snow Mass, Colorado, USA (August 2016) and during the Green House Gas Technology meeting (GHGT13) in Lausanne, Switzerland (November 2016).

TABLE OF CONTENTS

Page

Study of CO_2 foam performance in a CCS context

Guillaume Batôt[11], Chris Hewson[2], Lahcen Nabzar[1] , Marc Fleury[1]

[1]IFP Energies nouvelles, Rueil-Malmaison, France
[2]TNO, Utrecht, Netherlands

Submitted to International Journal of Green Gas Control 10/02/2017

Keywords: CO_2 storage, remediation, foam, apparent viscosity, NMR.

Abstract

As part of the MiReCOL three-year European project (www.mirecol-co2.eu) on storage remediation technologies, this work investigate the use of foam injected into the subsurface for the purpose of mitigating a CO_2 leak through the cap rock of a storage reservoir.

In the laboratory the capacity of foams to reduce gas flow was studied for CO_2-brine systems in rock core sample with common surfactants, as a function of interstitial velocity and gas to water fraction. The performance of the generated foams was evaluated from the relative foam viscosity, the ratio of the measured pressure drop in the presence of foam to the pressure drop in single phase condition for the same interstitial velocity. Whatever the pressure and permeability/porosity, the relative foam viscosity can be described as a power law vs. the shear rate evaluated from the interstitial velocity, permeability and porosity. The exponent is close to -1 describing the shear-thinning behavior.

Based on this experimental correlation the technical feasibility of foam injection, as a mitigation method, was numerically explored from reservoir simulations. Although foam injection reduce the rate of CO_2 leakage in order to allow for further remediation, but without gelation the method is a temporary solution when foam decay is taken into account.

[1] *guillaume.batot@ifp.fr*

1 INTRODUCTION

The oil and gas industry has a long-term experience in reducing the flow rate of a given fluid, or maximizing the oil and gas recovery, by injecting fluids with specific properties into rock formations containing hydrocarbons. As it has already been stated[1], Carbon Capture and Sequestration programs (CCS) could benefit from the CO_2-Enhanced-Oil-Recovery knowledge. Indeed, in the EOR context, the gas-based injections are now the most common methods since the decline of the thermal ones in the early 2000's[2]. Due to its unique properties such as low minimum miscibility pressure, CO_2 has been mainly used in such techniques.

Beyond their use for mobility control in EOR, foams can also be adequate to secure gas storage operations through gas confinement and leakage prevention/remediation. Regarding CO_2 storage operations, gas confinement is of great importance to ensure that such process can be used as a safe and effective solution for greenhouse mitigation. A clear insight on the associated risks, their sound evaluation and the development of means for their prevention and mitigation are thus needed. Risks of CO_2 leakage through/along wells, faults and fractures and through the sealing cap-rock are among the most important. Indeed, due to its low density and high mobility, gas might potentially migrate out of the storage zone towards the upper formation due to gravity segregation and finally might leak into the atmosphere. This leakage potential is mainly determined around the well and on the sealing cap rock integrity. Due to their ability to preferentially restrict fluid flow in the most permeable areas, foams are particularly indicated to address the leakage from high permeability areas or through fracture and fissures that are considered as the most important leakage pathways[3].

The foam lifetime in the porous media may be about few weeks, at best, thus the use of classical foams in a CCS context is adapt for emergency remediation but for mid-term prevention gel-foam[4] can be designed. For both, classical and gel foams, laboratory experiments in rock samples are based on the evaluation of the gas flow resistance of the foam lamellae. The gel-foam implies a complementary chemical study on the relevant cross-linkers needed to gel the foam. In the following we focus only on the foam generation, propagation, and its ability to reduce the gas flow rate in porous media.

1.1 Foam generation and propagation in porous media

Despite numerous theoretical studies[5,6], experimental works[4,7,8] and field/pilot tests[9–11] dedicated to foam processes, it is still a developing technology and uncertainties remains regarding the governing parameters of this complex physics. On several aspects, foams generated in rock formations are very different from the "everyday life" or "bulk" foam that we are familiar with. In porous media they can be seen as finely-textured gas bubbles, such as nitrogen, methane or carbon dioxide, dispersed within brine. Their formation requires a certain amount of energy, which is provided by shearing along the porous structure, and are stabilized by surfactants that are generally solubilized in the water, but could also be dissolved into the CO_2[12,13]. The gas bubbles are separated by liquid films called lamellae, responsible for the reduction of the gas

flow. In homogeneous structure, lamellae creation results from two main identified mechanisms[6]: the lamellae division and the gas bubble snap-off. A third mechanism is also identified, the leave-behind, but it can be seen as a specific case of the lamellae division. Thus, the gas transport properties may result from a dynamic equilibrium between lamellae creation and destruction.

At the laboratory scale, the resistance to gas flow, *i.e.* the resistance of the lamellae to coalescence, is evaluated macroscopically within rock core sample from the pressure drop ΔP_{foam} along the core. The so-called gas Mobility Reduction Factor (MRF) is defined as the following ratio $\Delta P_{\text{foam}}/\Delta P_{\text{ref}}$, which can be seen as a relative and apparent viscosity of the generated foam at a given flow rate. The reference pressure drop can be the water pressure drop (monophasic reference) or the pressure drop measured from a water and gas co-injection (diphasic reference).

In the absence of oil, the lamellae coalescence seems to be mainly governed by the capillary pressure P_c and the local water saturation S_w. Two regimes of foam flow have been distinguished[7] : in the P_c^* regime, when the P_c is close, or equal, to the limiting value P_c^*, the generated foam is "strong" and provides high MRF; below the P_c^* the foam is "weak" and does not give large resistance to gas flow. At a given total flow rate, the capillary pressure can be increased with the gas fractional flow, or foam quality, denoted as $f_g = \frac{Q_g}{Q_w+Q_g}$ the gas flow rate divided by the total flow rate. When the limiting capillary pressure P_c^* is reached, further increase in the foam quality induces instabilities through coarsening of the foam texture. There is an upper limit, mostly over f_g~0.9, above which foam collapses due to "dry out" effect.

In the P_c^* regime two flow regimes exist and the transition occurs at a critical or optimal gas fraction f_g^* corresponding to the critical capillary pressure and to the maximum in pressure drop at a given total flow rate. With low quality wet foam, $f_g < f_g^*$, the pressure drop is almost independent of the liquid flow rate while for dry foam at high quality, $f_g > f_g^*$ it becomes almost independent of the gas flow rate[14]. The optimal foam quality is usually obtained between 0.7 and 0.9[15]. Thus, according to this view, the foam-induced pressure drop usually exhibits a maximum when plotted against foam quality[15–18]. This maximum is reached at the optimal foam quality f_g^* that depends on system characteristics and especially on formation permeability, surfactant and flow rate. This optimal foam quality is a very important parameter to determine for a given application case.

It has been demonstrated that for strong foam generation, a minimum pressure gradient or a minimum critical velocity is required[4]. Once these strong foams are generated, inside the porous media, their rheological behavior shows the following main trends: first, MRF increases with increasing velocity up to a maximum. Then MRF decreases when increasing further the velocity beyond the maximum (shear thinning behavior). Finally, MRF shows hysteresis effect when the velocity is decreased. Such typical rheological behavior is illustrated on Figure 1.

Most of the foams exhibit the shear thinning behavior. This is an important advantage for the use of foams in EOR for sweep improvement. Indeed, foams are usually generated in situ in the near wellbore area where the velocity is high leading to low MRF that mitigate the injectivity issue. Far away from wellbore, the velocity decreases leading to higher MRF with better gas blocking performance.

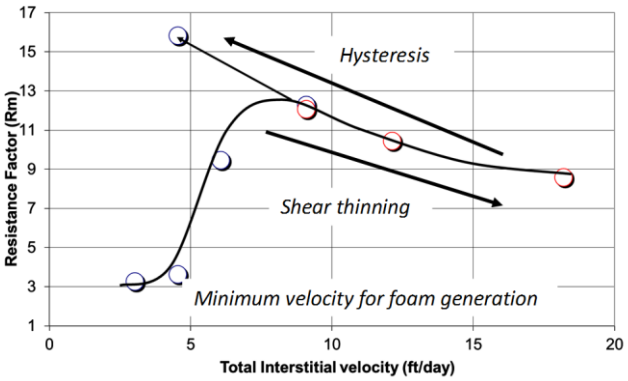

Figure 1: Typical behavior of foam when increasing the total interstitial velocity. Hysteresis may occur with decreasing velocity, yielding higher resistance to gas far from the well (Nabzar, 2014, ADRAC, Abu Dhabi). Conditions: 40°C, 130 bar.

1.2 Numerical simulation of foam

Empirical[19], semi-analytical[20,21] and mechanistic[22,23] approaches have been proposed to model foam flow in porous media[24]. The mechanistic models are based on the population balance equation taking into account lamellae creation and destruction in order to predict the dynamics of the foam bubbles. They aim at describing the relation between the space-time variation of the foam structure and its rheological properties. The use of such comprehensive models is however limited due to the number of parameters that are difficult to obtain, measure and scale-up at larger scale. The semi-analytical approach is based on the application of the fractional flow theory of Buckley-Leverett to foam flow[20,21]. Though such model is able to reproduce the general foam behavior described above, its use for foam is limited due to the assumptions used. Therefore, in the absence of a comprehensive, simple, yet useful, physical modeling of foam flow in porous media, only the empirical approach, is currently used in most of the reservoir simulators. Within this approach, based on the local steady state model, the effect of foam on gas mobility is modeled through a simple modification of the relative gas permeability k_{rg} in presence of foam k_{rg}^{f} :

$$k_{r,g}^{f} = k_{r,g} M_{rf} \tag{1}$$

The mobility reduction factor M_{rf} are input values obtained from the experimental measurements. A functional form or a tabular form can be use depending on the available data.

2 MATERIAL AND METHODS

2.1 Core-flood experiments

Experiments presented in this work were carried out in Clashach sandstones with a water permeability between 225 mD and 1550 mD and a porosity between 10% and 20%. Depending on the experimental set-up, two different plug sizes are used, the smallest ones have a pore volume of 1.5 and 2.5 ml with a length of 4.0 cm and a radius of 1.0 cm, while the largest has a pore volume of 25 ml with a length of 10.0 cm and a radius of 2.0 cm. The water used is a 3.5wt% NaCl brine. Surfactant is a classical AOS type (Rhodacal® A-246/L manufactured by Solvay) prepared at the concentration of 0.5 wt. % in this brine.

A typical experiment consists in first co-injecting brine and pure CO_2, and then brine is replaced by a solution of the same brine but containing a surfactant. In all these experiments CO_2 and surfactant-brine are co-injected at the core inlet to make sure that the foam is generated by shearing through the porous structure, and not before. The foam quality f_g, or gas fraction, is fixed around 0.7. Various total flow rates varying from near wellbore to in depth fluid velocities can be explored in an experiment.

2.1.1 MRI system at low pressure

With the MRI small core-flood set-up (Figure 2), brine and pure CO_2 are co-injected at the top inlet face of the sample. The flooding cell is custom built and specifically designed for MRI systems: sample diameter is 2.0 cm with a maximum sample length of 5.0 cm; NMR probe diameter is 3.0 cm; the maximum confining pressure is 80 bar and 10 bar pore pressure is imposed by a membrane back-pressure regulator (BPR); the temperature is fixed around 30°C (MRI magnet temperature). The liquid and gas flow rates are respectively imposed using a pump (QX-6000 from Quizix) and a gas controller (EL-Flow® from Bronkhorst®). We vary the total flow rate Q_t by a factor of 100, from 1 cm^3/h up to 100 cm^3/h, corresponding in this case to interstitial velocity $v_i = Q_t/(S\phi)$ between 1.6 and 160 cm/h, or between 1.22 and 122 ft/day in usual engineering units. During injection, we continuously measure by standard MRI techniques the saturation profiles (a spin echo sequence) and the T_2 relaxation time distributions typically every minute.

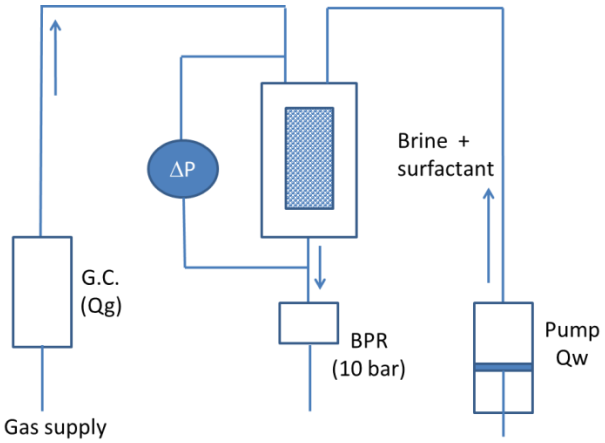

Figure 2: Schematic of the experimental set-up using NMR imaging. Gas controller (G.C.) to impose a fixed gas flow rate. Back pressure regulator (BPR): used to set the outlet pressure. The MRI system is a 20 MHz compact permanent magnet system from Oxford Instrument.

2.1.2 X-Ray system at high pressure

The high pressure system is conceptually similar and is composed of a horizontal composite core holder with low X-ray attenuation. The X-ray generator (90keV – Ta filter) and the detector can move along the heated Hassler cell using a step by step motor. A full-length scan every 5 mm takes about 15 min. A saturation profile is calculated from the measured X-ray profile and two calibration profiles (sample fully saturated with brine and dry). The CO_2 is injected from a high pressure piston-cylinder cell at the chosen working pressure and temperature; experiments were carried out at 40°C and 130 bar pore pressure with 180 bar of overburden pressure; the core sample used had a water permeability of 820 mD and a porosity of 20.2 %. The total flow rate was changed from 10 to 300 cm^3/h yielding interstitial velocities between 3.9 and 119.3 cm/h (3.1 and 94.0 ft/day) in the same range as in the MRI setup. At 40°C and 130 bars, the injected CO_2 is in a supercritical dense state with a density of 743 ± 3.7 kg/m^3 (from NIST database).

2.2 Numerical simulation

The technical feasibility of foam injection as a remediation method was explored using Schlumberger's commercial reservoir simulator Eclipse 100.

2.2.1 Reservoir model

A reservoir model was created to study the mobility control of CO_2 with the use of a foam in a depleted gas field considered for CO_2 storage (P18-4[25]). The model was purposely simplified and was created with similar properties.. The structural model was a tilted box (10º dip) so that the gravity effects of the fluid could be studied. The bounds were no flow boundaries to emulate the P18-4 field compartments. The extent of the model was 1075 m x 1925 m x 130 m with a grid block size of 25 m x 25 m x 5 m (x, y, and z direction respectively) as to not have the bounds interfere with the determination

of the radius of investigation. The injection well was perforated in the top 50 m of the reservoir (Figure 3). The relatively high resolution of the model was used to properly model the dispersion of the foam. The permeability field was chosen to be homogenous with 200 mD in the horizontal direction and 20 mD in the vertical direction. The porosity was also homogenous throughout the reservoir and was chosen as 0.15.

For this study, the overburden was not considered. Instead a production well was used to model the effect of a leakage zone in the cap rock. The size of the leak in the reservoir section was chosen as 2 m x 2 m x 25m. It was assumed that the cap rock would leak after the reservoir pressure reached 400 bars (reactivation pressure).

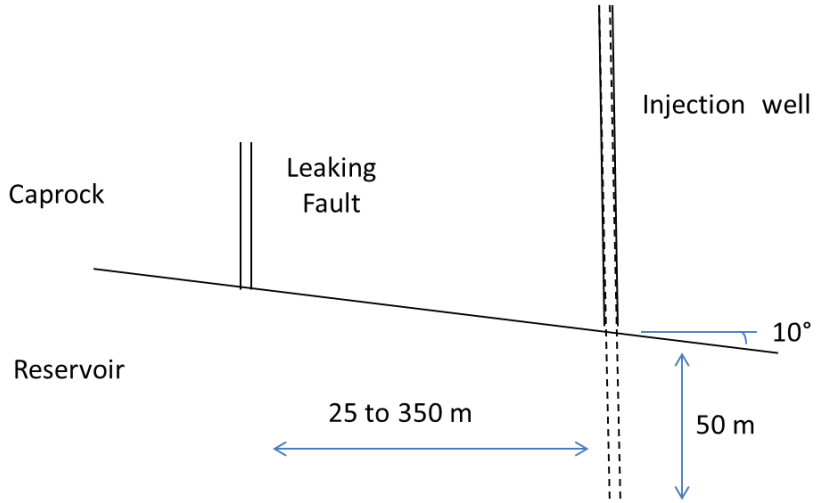

Figure 3: sketch of the injection well and leaky fault in the caprock. The injection is perforated over the top 50m of the reservoir. The distance between the well and leaking fault was varied from 25 up to 350m.

The leakage through the cap rock (i.e. leak well) was under rate control with a minimum pressure limit of the aquifer above (we assume that at that point no more CO_2 can leak from the reservoir). The parameters used to model the leak are presented in Table 1. Additionally, a rate control was imposed on the leak using a combination of Buckingham's equation[26] for flow through slots of fine clearance (eq. 3) and Darcy's law (eq. 2) :

$$q_f = -\frac{k_f A}{\mu}\left(\frac{\Delta p}{L}\right) \tag{2}$$

$$k_f = \frac{\phi_f w_f^2}{12\tau} \tag{3}$$

where

Δp = differential pressure [Pa]
k_f = fracture permeability [m^2]
μ = fluid viscosity [Pa*s]

L = length of fracture (i.e. thickness of the caprock) [m]
A = cross-sectional area [m^2]
q_f = volumetric flow rate through fracture [m^3/s]
ϕ_f = fracture porosity [-]
w_f = fracture width [m]
τ = fracture tortuosity [-]

Table 1 – Parameters values for the leak model.

Fracture Permeability [D]	29
Length of Fracture [m]	20
Cross-sectional Area [m^2]	0.01181
Fracture Porosity [-]	0.43
Fracture Width [m]	0.000009
Fracture Tortuosity [-]	0.01

The implementation of two separate operating constraints for the leak allow for sufficient modelling of the leakage zone without the inclusion of a complex geological model or a large fracture extent. The leak permeability was taken to be 29 D, correlating to a leak flow rate of approximately 200 kg/day. The leakage rate was chosen based on a worst case scenario cap rock failure and was checked for a basis in reality from a previous study on CO_2 leakage from geological storage[27].

2.2.2 Transport equation

The commercial reservoir simulation software, Schlumberger's Eclipse 100, was used to model the depletion of the gas field, injection of CO_2, the leakage of CO_2 from the reservoir, and the injection of foam to mitigate the leak. The foam is modeled as a tracer in the gaseous phase of the reservoir simulator. The foam can be thought of as being dependent on the surfactant concentration that exists in foam form. The simulation software models the amount or concentration of surfactant that is able to reach different points of the reservoir (in terms of both flow and degradation effects) and directly relates this to a parameter known as foam concentration. A conservation equation is used within Eclipse to determine the concentration of the activated surfactant in each grid block (in the numerical simulator's conservation equation this is referred to as the foam concentration). The mobility reduction factor, M_{rf}, is introduced into the local conservation equation (without adsorption effect) for the gas phase and is shown in equation 4:

$$\frac{d}{dt}N_f = \sum\left[\frac{Tk_{r,g}}{\mu_g}M_{rf}\left(\delta P_g - \rho_g g D_z\right)\right]C_f + Q_T f_g C_f \qquad (4)$$

with N_f the number of foam tracers in a simulation block, C_f is the foam concentration, ρ_g the gas density, T the absolute permeability (transmissivity), P_g the gas pressure, g the gravitational constant, D_z the cell center depth, Q_T the total flow rate, and f_g is the

gas fractional flow. The summation is performed over all neighboring cells in 3 dimensions.

Foam propagation using numerical simulators has been well documented in previous studies[19,24,28]. Eclipse uses a set of user defined parameters to model transport, adsorption, decay and the mobility reduction factor M_{rf}. The gas mobility reduction can be calculated either using tables or functional parameters. In this work, the tabular model was chosen as we can use the M_{rf} obtained from the corefloods experiments as direct input. The tabular model includes surfactant concentration, pressure, and shear dependent terms. Equations 5 and 6 display the equations Eclipse uses to determine the mobility reduction factor (M_{rf}) of the foam:

$$M_{rf} = \left(1 - M_{rf}^{cp}\right) M_v\left(V_g\right) + M_{rf}^{cp}, \tag{5}$$

$$M_{rf}^{cp} = \left(1 - M_c\left(C_f\right)\right) M_p(P) + M_c\left(C_f\right), \tag{6}$$

where $M_v(V_g)$ is the mobility reduction modifier due to interstitial velocity, $M_c(C_f)$ is the gas mobility reduction modifier due to the foam concentration and $M_p(P)$ is the gas mobility reduction modifier due to pressure. The foam does require a minimum concentration of 0.05 to be effective, below that concentration in a grid block, the foam begins to collapse. In our modeling, foam does not degrade over time and the surfactant does not adsorb on the surface of the rock. This assumption is not always verified, especially in the presence of hydrocarbons and biological impurities within the rock matrix[29,30]. Hence, we consider an ideal foam with the objective of studying the main mechanisms.

3 RESULTS

3.1 Low pressure system: transient regime before foam formation

Here we focus on the onset of foam at the lowest flow rate (1 cm^3/h or 1.6cm/h, Figure 3). The sample is a Clashach sandstone of porosity 20.2% and water permeability 1550 mD. The sample was used for several foam experiments before this one and therefore adsorption of the surfactant on the solid surface is stabilized. A foam generating a strong pressure drop is only observed when the water saturation is low enough (~15%), corresponding to high capillary pressure close to irreducible water saturation (Figure 3 – left). This is achieved after a few pore volume (PV). Then, at a nearly constant water saturation and during a few pore volume also, a strong foam is abruptly formed as indicated by the sharp increase of the pressure drop after injection of 2 PV or at this low flow rate after t= 6.2 hr. Interestingly, the saturation profiles (Figure 3 - right) are nearly uniform for strong foams and this uniform profile is gradually achieved starting from the middle of the sample.

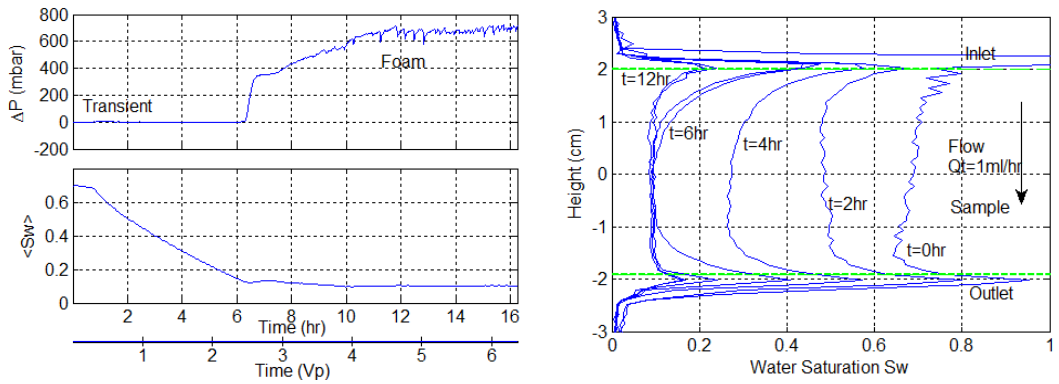

Figure 4: [Left] Generation of foam at a low interstitial velocity (1 ml/h, 1.6 cm/h) : Clashach sandstone, porosity 20.2%, 1550 mD, f_g=0.6, brine 35 g/l, AOS type surfactant concentration 0.5 wt%.[Right] Local saturation profiles corresponding to the left graph every 2 hours. At t=6 hr, a strong foam is present. The spikes at the inlet and outlet correspond to the liquid present in the injectors. The average saturation is calculated with the values between the green horizontal lines.

3.2 Low pressure system: foam apparent viscosity

At steady state, the mobility reduction factor is calculated as the ratio of the measured pressure drop in the presence of foam $\Delta P_{foam}(Q_t; f_g \sim 0.7)$ to the one during a single phase brine injection $\Delta P_{brine}(Q_t)$ at the same total flow rate Q_t:

$$MRF(Q_t; f_g) = \frac{\Delta P_{foam}(Q_t; f_g \sim 0.7)}{\Delta P_{brine}(Q_t)}. \quad (7)$$

Indeed, as shown by 3D CT-scan imaging[8], defining the mobility reduction factor with the pressure drop in two phase flow conditions (co-injection of gas and brine without surfactants) in such short samples has little meaning due to severe digitation problems. Based on the Darcy law, with this definition the MRF can be seen as the foam relative

apparent viscosity, denoted as η_r^f in the following, which corresponds to the ratio of the foam apparent viscosity to the brine viscosity $\eta_{\text{app}}^f / \eta_{\text{brine}}$.

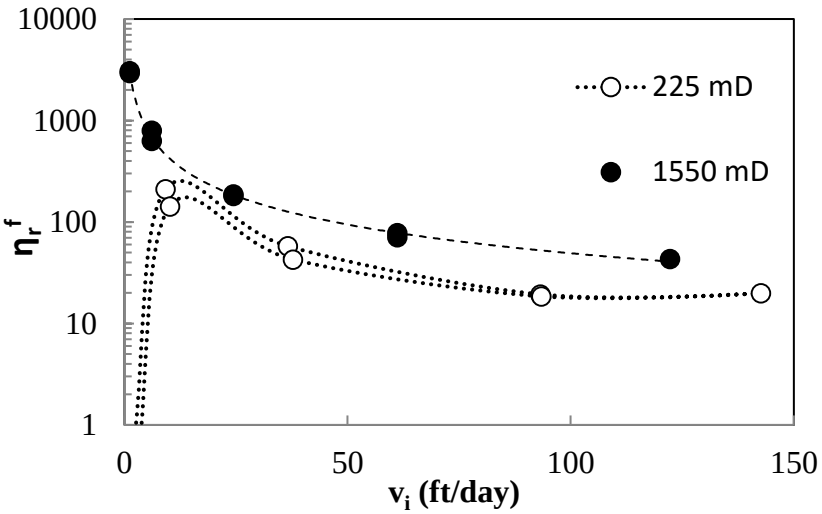

Figure 5: Foam relative viscosity in a small core of Clashach sandstone plotted against the interstitial velocity. Full circles correspond to the date obtain with a core of 1550 mD water permeability and 20.2% of porosity. Empty circles are the data for 225 mD and 12.1% porosity. Points are obtained with both increasing and decreasing velocities (duplicate points).

On Figure 5 the foam relative viscosity η_r^f is plotted against the total interstitial velocity for the two permeability values. The data obtained from increasing and decreasing total flow rate are very similar (duplicate points). In the less permeable rock sample, at the lowest interstitial velocity of 2.2 ft/day, the measured apparent viscosity is very close to 1, suggesting that there is strictly speaking no foam generated at this point. At 9.2 ft/day we observed a rise of the pressure drop and strong water desaturation of the porous media, leading to a relative viscosity about 100-200. No such critical velocity is observed with the more permeable core, as it may be too small to be measured with the present experimental set-up.

3.3 High pressure system: foam apparent viscosity

The flooding cell used with the high pressure setup allows working with longer core sample (10 cm) and denser gas. Hence, we first measured reference pressure drops when water and CO_2 are simply co-injected without any surfactant for a range of velocities used later in the presence of foam (Figure 6). The data are well described by linear relationships and both linear regressions can be used to evaluate either the performance ratio between foam and gas/water co-injection MRF $= \Delta P_{\text{foam}} / \Delta P_{\text{water-gas}}$, or the relative foam viscosity $\Delta P_{\text{foam}} / \Delta P_{\text{water}}$.

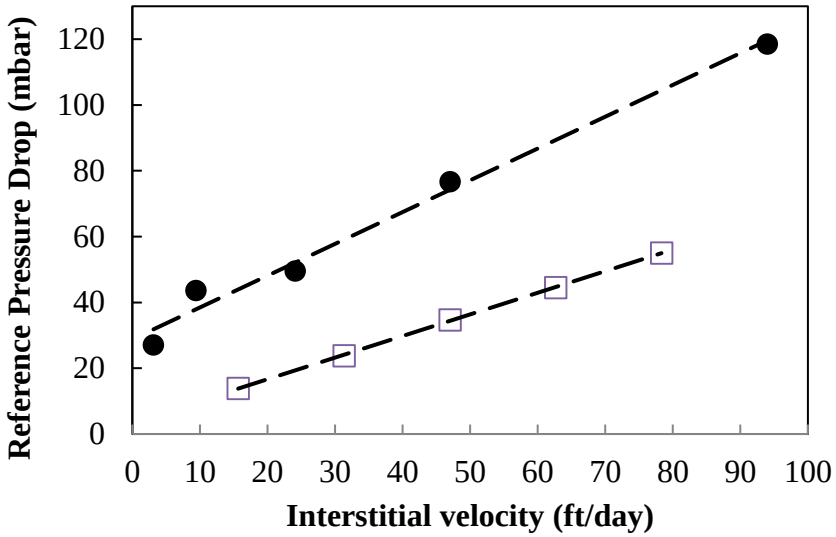

Figure 6: Pressure drops for several interstitial velocities. Empty squares are the measurements from the injection of water without surfactants, while the full circle from the co-injection of gas and water still without surfactants. Dotted lines are linear regressions.

During the foam generation and propagation in the porous media, the mean water saturation is recorded from X-ray absorbance technique. During the first four injected pore volumes, at the total flow rate of 10 cm^3/h (or 3.1 ft/day interstitial velocity), the transient regime of the initial foam formation is clearly observed and correlated to a fast water desaturation (Figure 7). Increasing the total flow rate increases the pressure drop as expected if the foam still exists and does not coalesce.

When scaled by the water-gas pressure drop at the same velocities (Figure 6), the MRF does not express anymore a relative viscosity (Figure 8) but the “true” effect of the foam compared to a situation in which both gas and water are flowing in the absence of foam (i.e. it includes relative permeability effects). Then, the mobility reduction factor ranges between 20 and 50 with a less pronounced shear thinning evolution.

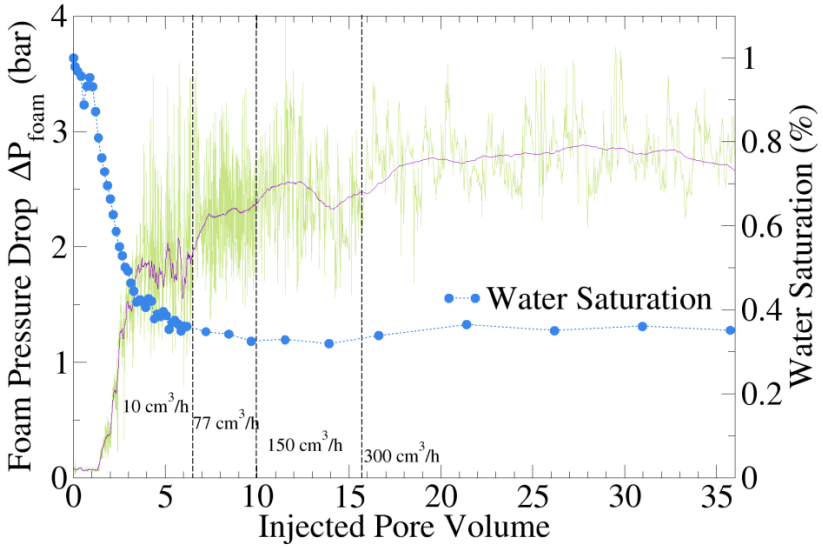

Figure 7: Dense supercritical CO_2-foam generation in a 820 mD Clashach sandstone. The line in dark purple is a running average of 200 points of the raw pressure drop measurement represented here in light green. The full circles represent the mean water saturation along the core. Data are plotted against the total injected pore volume and thus not linear in time as the total flow rate was increased from 10 up to 300 cm^3/h.

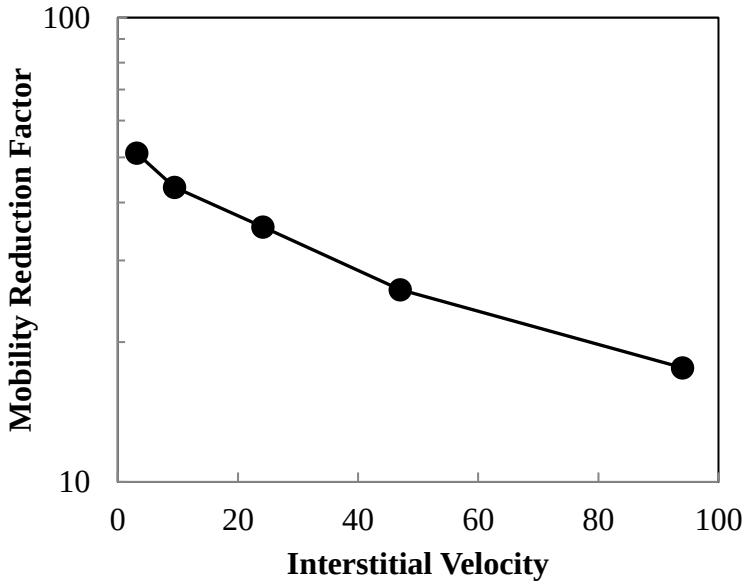

Figure 8: Mobility Reduction Factor evaluated from the performance ratio between foam and gas/water co-injection $MRF = \Delta P_{foam}/\Delta P_{water\text{-}gas}$. The $\Delta P_{water\text{-}gas}$ is extracted from the linear regression of raw data (Figure 6).

3.4 Synthesis

As the interstitial velocity takes into account the porosity, it is not an adequate variable to compare results between plugs with different porosity but having the same permeability. We suggest to use the shear rate noted $\dot{\gamma}$ which is however not a quantity directly available from measurements in complex geometries. The shear rate is critical for polymer systems flowing in porous media and an empirical law has been established by Chauveteau[31] in sandstones and bead-packs. Very recently Pedroni[32] have shown that this law can be successfully used for foam flow in homogeneous sandstones. From a classical rheological point of view the Chauveteau law can be expressed as follow:

$$\dot{\gamma} = 4\frac{v_i}{l_s}\alpha(K_w) \qquad l_s = \sqrt{8K_w/\Phi} \qquad (8)$$

with v_i the interstitial velocity, l_s the typical length scale of the sheared zone and α an empirical correction which is a decreasing function of the water permeability K_w. The length l_s is the pore throat estimated from conduit flow model as $\sqrt{8K_w/\phi}$. Extrapolating the relation $\alpha = 16.71\times {K_w}^{-0.277}$ from the data obtained by Chauveteau et al.[31], we found $\alpha \simeq 3.7275$ for 225 mD and $\alpha \simeq 2.189$ for 1550 mD. Plotting the foam apparent viscosity against the shear rate calculated with the above coefficients yields a unique curve (Figure 9). Thus the data obtained from different permeability and porosity are reduced to a single power law curve with exponent close to -1 (between -0.90 and -0.95).

The water saturation (also plotted on Figure 9) increases monotonously, from 10 to 20%, as the foam relative viscosity decreases with the shear rate. As η_r^f decreases the foam becomes less effective in reducing the CO_2 flow and the gas may flow more easily along the preferential paths, resulting in an increase of the water saturation. Furthermore one could also observe that water saturation is always below the injected water fraction $f_w = 1 - f_g = 30\%$. It means that the gas mobility is well reduced within the rock and the generated foam is very efficient for the whole range of interstitial velocity used here: from 3 ft/day to 100 ft/day, representative range from in depth fluid velocities to near wellbore.

Performing the same analysis for the high pressure data, the shear rate $\dot{\gamma}$ was estimated from eq. 8 with $\alpha = 2.605$ for $K_w = 820$ mD and $\phi = 20.0$ %. We observed that the foam relative viscosity η_r^f can be described with the same power law for both low and high pressure measurements (Figure 10). The exponents are respectively -0.94 and -0.92 for the low and high pressure conditions. Thus, at steady state, the generated CO_2-foam shows the same ability to reduce the gas flow, whatever the pressure.

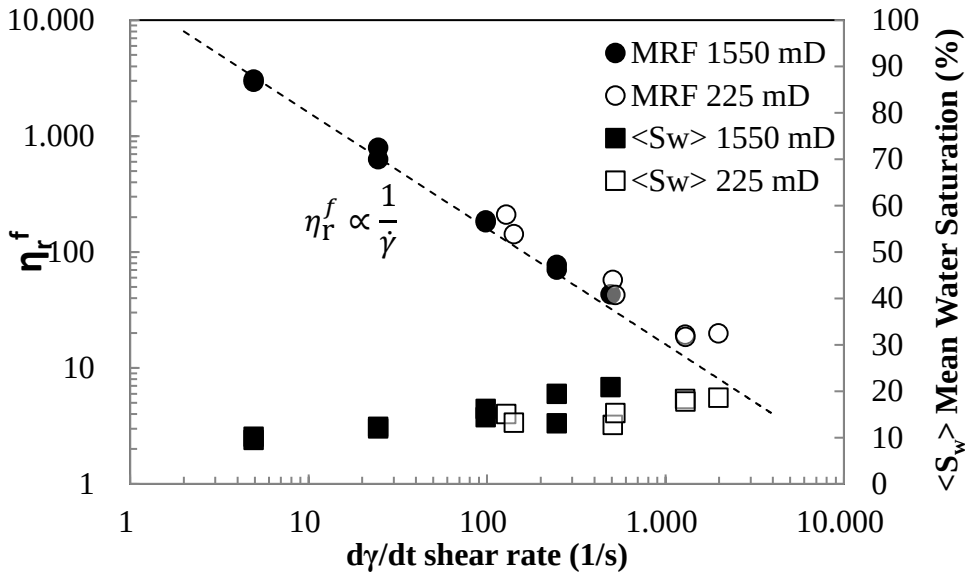

Figure 9: The foam relative viscosity η_r^f (circles) and the mean water saturation <S_w> (squares) vs. the shear rate $\dot{\gamma}$ computed from eq. 8 in Clashach sandstone at 30°C and a pore pressure of 10 bar. The full symbols represent data for a 1550 mD sandstone with a porosity about 20%. The empty symbols for 225 mD with a porosity about 12%. The dotted line corresponds to the equation $\eta_r^f = 16000/\dot{\gamma}$.

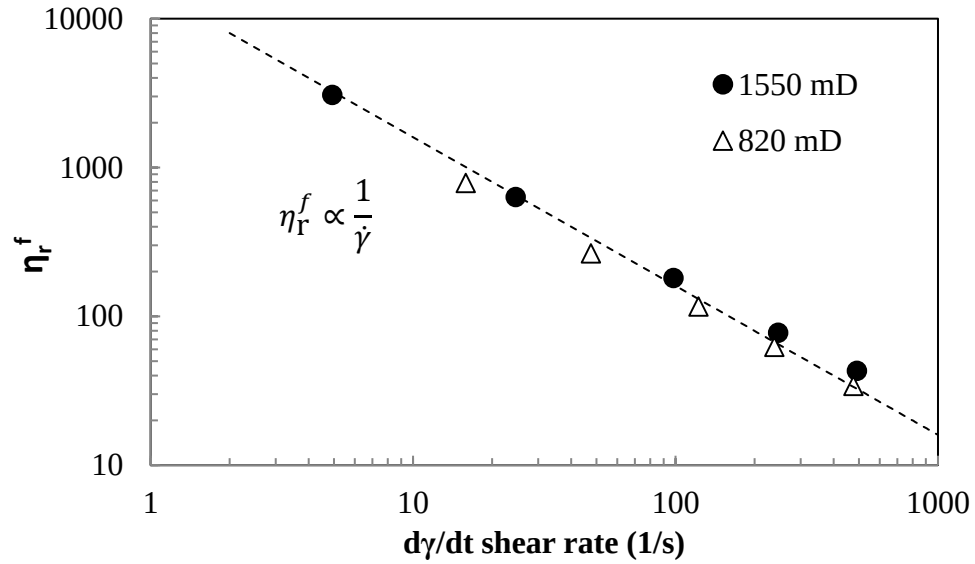

Figure 10: Comparison between low (full circle - 1550 mD) and high pressure (empty triangles - 820 mD) experiments for the decreasing velocities (as in reservoir application). The shear rate is computed from eq. (8**Error! Reference source not found.**. The dotted line is the same power law as plotted on Fig. 8 : $\eta_r^f = 16000/\dot{\gamma}$.

The effective viscosity of the foam can finally be modeled for all conditions as a function of the shear rate (eq. 8) according to:

$$\eta_r^f = \frac{16000}{\dot{\gamma}} \tag{9}$$

in which we impose an exponent -1 close to the measured ones. This relation includes the effect of permeability and porosity and can be used for foam simulations. Indeed, for a given formation of permeability K and porosity Φ, one can calculate the velocities according to equation 8, and the effective foam viscosity function of velocity according to equation 9. Hence, the MRF curve function of velocity can be entered as input parameter, as shown later.

3.5 Foam Simulations : Radius of Investigation

Since the relationship in equation 9 cannot be entered directly as an input in the simulator, the tabulated values $M_v(V_g)$, $M_c(C_f)$, and $M_p(P)$ were first adjusted in order match the experimental pressures and saturations observed, i.e. the foam effective viscosity follows a power law function of total interstitial velocity. Since the experiments show no pressure effect, the foam pressure parameter (M_p) takes a very small value. However, Eclipse does not allow for MRF values to increase with increasing shear rates and hence, the typical foam behavior shown in Figure 1 with the inflection point cannot be explicitly modelled in the simulator.

The radius of investigation was looked at to determine how far the foam could reach a leak in the cap rock. Leak distances of 25 m, 75 m, 175 m, and 350 m from the injection well location were looked at to determine the time of intervention and the volume of foam that was able to reach the site relative to the injected volume of foam. A surfactant-alternating-gas (SAG) process was used to generate the foam in situ. For our study, one slug of surfactant solution was injected at a rate of 100 m^3/day for 2 months, followed by a CO_2 gas slug of 200 t/day for 3 months in order to prevent injectivity issues of surfactant and gas around the near wellbore region.

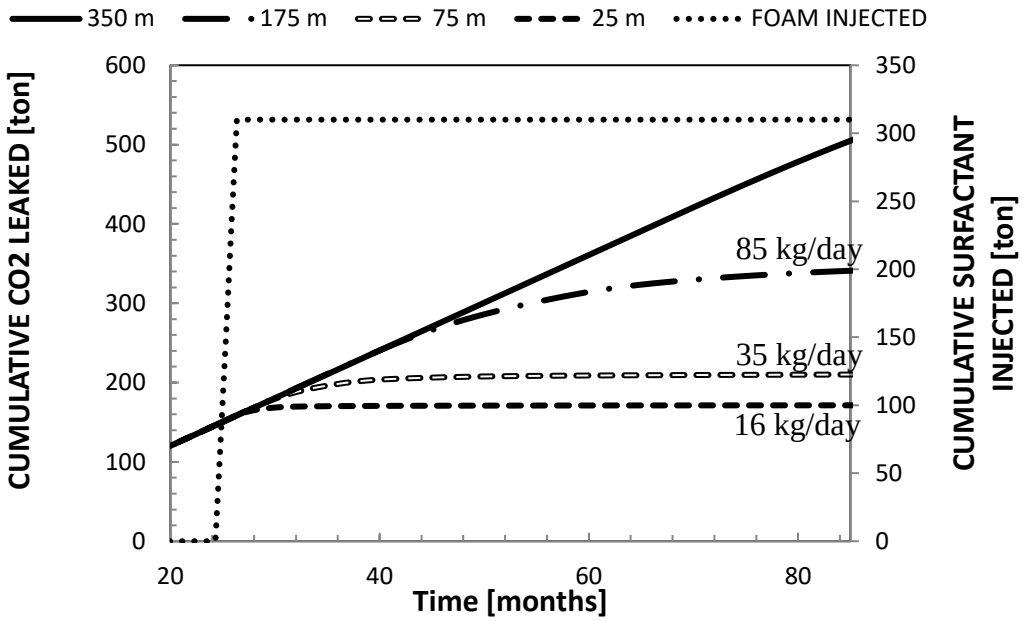

Figure 11: Cumulative CO_2 production through the leak at various distances from the injection site. The dotted line indicates the start of surfactant injection into the reservoir. The final CO2 leak rate obtained at the end of the simulation is indicated near the corresponding curve, it should be compared to the initial value of 200 kg/day.

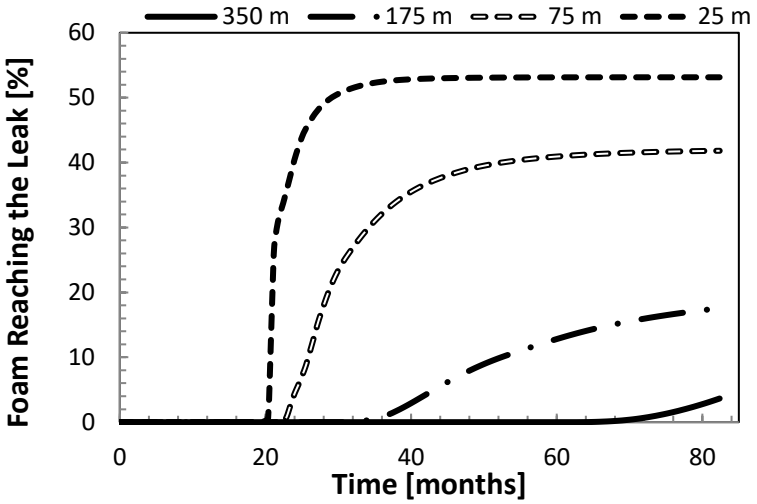

Figure 12: Cumulative percentage of injected foam (injection period of 180 days) reaching the leak location with varying distance from the foam injection location.

As the leak distance increases, the amount of CO_2 that can be prevented from leaking decreases (Figure 11). The leak rate decreases from the initial value of 200 kg/day down to 16, 35 and 85 kg/day respectively for distances of 25, 75 and 175m. As well, the amount of the surfactant and gas mixture and the time at which the foam reaches the leak location is greatly affected by the distance of the injection well from the leak. The percentage of injected foam contacting the leak site is shown in Figure 12. The amount of time that it takes for the foam to have an effect on the CO_2 leakage for the 175 m case

(500 days) makes the foam mitigation technique ineffective as it requires such a large amount of time. Figure 12 shows that a low percentage of the foam has actually reached the leak. The rest of the foam has spread itself throughout the reservoir as there is no way to direct the foam to the leak site. Not only does the foam have a larger distance to travel for the 175 m leak distance, but the plume of foam is also much wider in such a case. More foam is thus transported to parts of the reservoir/cap rock that do not benefit from the mobility reduction provided by the foam. The minimum shear velocity is not always satisfied for all cases, the only really effective case was seen in the 25 m distance scenario presented in Figure 13. We present the foam and shear rate 6 years after the end of injection for highlighting more clearly the foam flow but it is not expected that the foam would last for such a large duration. Although the minimum velocity condition for foam is not always satisfied when being transported to the leakage site (Figure 13 (c) and(d)), the velocity caused by the high flow rate at the leak site allow for the foam to be regenerated at the site of the leak if it had collapsed previously. The spread of the foam (Figure 13(a) and (b)) show that the foam is able to spread in the lateral directions in order to prevent further CO_2 leakage from occurring.

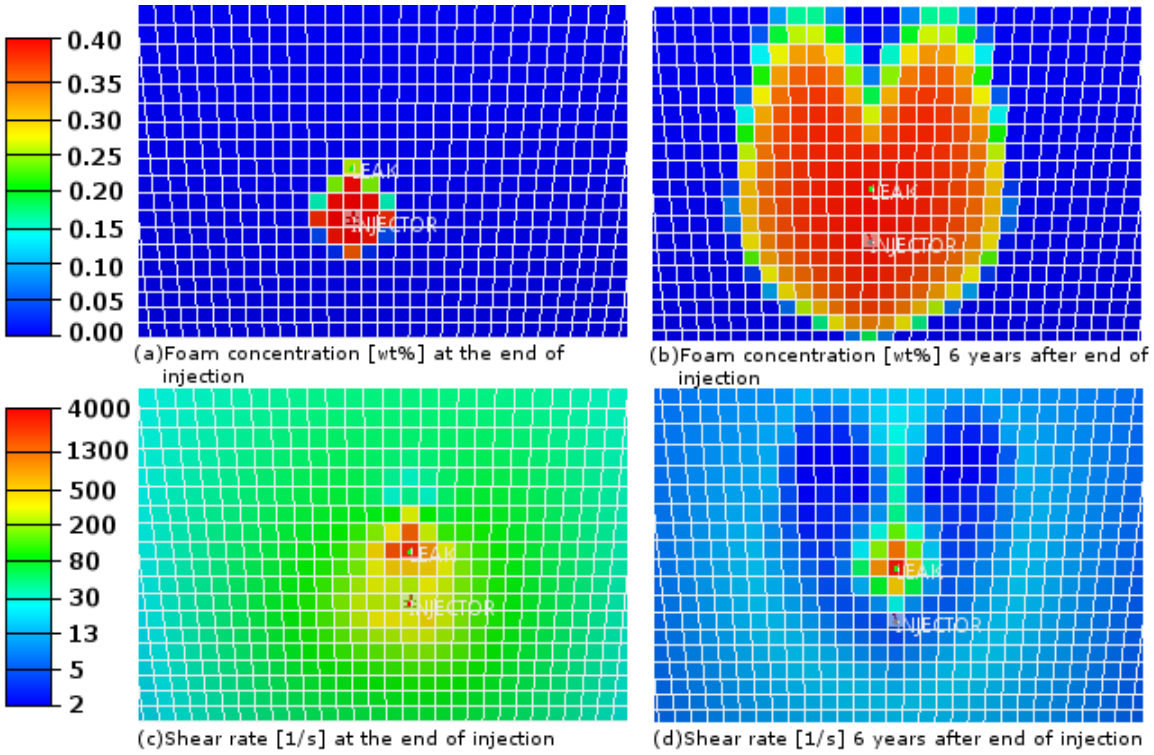

Figure 13: Comparison of the interstitial velocity and foam concentration for the 75 m leak distance situation in the grid block of the leak location.

At 25 m, the CO_2 leakage was reduced to a very low rate (16 kg/day) and rather quickly (31 days from the start of foam injection). The foam injection can be tailored for different leakage scenarios in order to effectively mitigate a leak with different parameters.

4 DISCUSSION

Using foam injection, the leakage of CO_2 was reduced in a relatively short amount of time as shown in Figure 10. This shows promising results for leaks that are relatively close to the injection well site. With large distances (greater than ~150 m), it is very difficult to reach the leak site as the foam will spread in all directions and will require large volumes of foam to reach the leak site in a realistic amount of time. Previous works[33] investigated using a hydraulic fracture to better transport a substance to the leak site, where a more concentrated solution could be placed at the leak site, which would overcome this issue of spreading.

The ability of the foam to flow and reach the leak site is greatly improved for a high permeability reservoir and it is more likely that the foam would flow to the leak due to the pressure gradient in the leak being encountered further from the leak site. In terms of controllable factors, the amount of foam injection added the greatest benefit for leak mitigation as the leaked foam would be replenished by the extra foam that was injected.

Similar to what was seen in previous literature[34,35], the leak was able to be slowed by the foam injection due to the reduced gas mobility induced by the foam. The effectiveness of this foam injection is highly dependent on the ability of the foam to reach the leak site and to do so in a reasonable amount of time. Foam injection is also a temporary solution, as the real situation would exhibit foam degradation over time. Additionally, foam will leak through the leak in the same manner as CO_2 would. The CO_2 would in essence be replaced with the foam leaking through the cap rock, potentially creating more problems than it has solved. The use of a gel-foam could be a solution to this problem, but the strength and stability of this substance should be investigated further, as well as the chemical interactions between all components. Considering the large quantities injected, the surfactant contained in the foam should be considered for potential environmental impact and weighed against the impact of CO_2.

5 CONCLUSIONS

We studied the performance of CO_2 foams as a mean to reduce the gas flow rate in the vicinity of fractures or reactivated faults in the context of CO_2 storage. The laboratory experiments were conducted on typical sandstones representative of storage formations, with permeabilities in the range 200-1500 mD, and porosities between 10 and 20 %. The surfactant-brine solution and the CO_2 were co-injected at the inlet face of the sample using two different set-ups, in which the local saturation profiles are measured either by magnetic resonance imaging or by X-ray attenuation. These set-ups allowed observing the onset of foam as a function of interstitial velocity, in the largest possible range from about 3 ft/day up to 100 ft/day. The performance of the generated foams was evaluated from the relative foam viscosity corresponding to the ratio of the measured pressure drop in the presence of foam to the pressure drop in single phase condition for the same interstitial velocity. Whatever the pressure and permeability/porosity, the relative foam viscosity can be described as a power law vs. the shear rate evaluated from an empirical law established for polymer systems in which the interstitial velocity, permeability and porosity are the main variables. The exponent is close to -1 describing the shear-thinning behavior.

By using foam injection in reservoir simulations, it was shown that the rate of CO_2 leakage could be significantly slowed in order to allow for further remediation. Assuming an ideal foam (no adsorption, no degradation over time), a typical radius of investigation is 50 m. For field applications, it is unlikely that the precise leak location would be known. Hence, the radius of investigation for treatment thus becomes an important parameter to consider when designing the foam mitigation technique. The maximum distance to be considered for the leak location thus becomes more important than the precise leak location in order for the injected foam to reach the leak. Since a large quantity of CO_2 is injected to create the foam and reach the leak location, another remediation method should be applied in the long term. From this point of view, we believe that a gel-foam would be more appropriate for mid-term remediation.

6 ACKNOWLEDGEMENTS

We acknowledge Solvay for providing the surfactant used in this study. Research in this paper was conducted with funding from the European Commission FP7 project MiReCOl, Grant Agreement n°608608.

7 REFERENCES

(1) MIT Energy Initiative Symposium. Role of Enhanced Oil Recovery in Accelerating the Deployment of Carbon Capture and Sequestration **2010**.
(2) Thomas, S. Enhanced Oil Recovery - An Overview. *Oil & Gas Science and Technology - Rev. IFP* **2008**, *63* (1), 9–19. DOI: 10.2516/ogst:2007060.
(3) Damen, K.; Faaij, A.; Turkenburg, W. Health, Safety and Environmental Risks of Underground Co2 Storage – Overview of Mechanisms and Current Knowledge. *Climatic Change* **2006**, *74* (1-3), 289–318. DOI: 10.1007/s10584-005-0425-9.
(4) Gauglitz, P. A.; Friedmann, F.; I. Kam, S.; R. Rossen, W. Foam generation in homogeneous porous media. *Chemical Engineering Science* **2002**, *57* (19), 4037–4052. DOI: 10.1016/S0009-2509(02)00340-8.
(5) Kovscek, A. R.; Patzek T. W.; Radke, C. J. Mechanistic Prediction of Foam Displacement in Multidimensions: A Population Balance Approach **1994**, SPE/DOE 27789.
(6) Dicksen Tanzil, George J. Hirasaki, Clarence A. Miller. Conditions for Foam Generation in Homogeneous Porous Media.
(7) Khatib Z.I.; Hirasaki, G. J.; Falls A. H. Effects of Capillary Pressure on Coalescence and Phase Mobilities in Foams Flowing Through Porous Media. *SPE Reservoir Engineering* **1988**, 919–926.
(8) Batôt, G.; Fleury, M.; Rosenberg E.; Nabzar, L.; Chabert, M. Foam Propagation in Rock Samples: Impact of Oil and Flow Caracterization. *SPE EOR OGWA Oman* **2016**, *SPE-179855-MS*.
(9) Skauge, A.; Aarra, M. G.; Surguchev, L.; Martinsen, H. A.; Rasmussen L. Foam-Assisted WAG: Experience from the Snorre Field. *SPE/DOE IOR* **2002**, SPE 75157.
(10) W.R. Brock, L.A. Bryan. Summary Results of CO2 EOR Field Tests, 1972-1987 **1989**.
(11) Enick, R. M.; Olsen D. K. Mobility and Conformance Control for Carbon Dioxyde Enhanced Oil Recovery (CO2-EOR) via Thickeners, Foams, and Gels - A detailed Literature Review of 40 years of Research. *DOE/NETL-2012/1540* **2012**.
(12) Bernard G.G.; Holm L.W. Method for recovering oil from subterranean formations **1967**, *US patent 3 342 256*.
(13) McLendon, W. J.; Koronaios, P.; Enick, R. M.; Biesmans, G.; Salazar, L.; Miller, A.; Soong, Y.; McLendon, T.; Romanov, V.; Crandall, D. Assessment of CO2-soluble non-ionic surfactants for mobility reduction using mobility measurements and CT imaging. *Journal of Petroleum Science and Engineering* **2014**, *119*, 196–209. DOI: 10.1016/j.petrol.2014.05.010.
(14) W.T. Osterloh and M.J. Jante Jr. Effects of Gas and Liquid Velocity on Steady-State Foam Flow at High Temperature **1992**, SPE/DOE 24179.
(15) J.M. Alvarez, H.J. Rivas, and W.R. Rossen. Unified Model for Steady-State Foam Behavior at High and Low Foam Qualities. *SPE journal* **2001**, SPE 74141.
(16) Chabert M.; Morvan M.; Nabzar, L. Advanced screening technologies for the selection of dens CO2 foaming surfactants **2012**, SPE 154147.
(17) Ma, K.; Lopez-Salinas, J. L.; Puerto, M. C.; Miller, C. A.; Biswal, S. L.; Hirasaki, G. J. Estimation of Parameters for the Simulation of Foam Flow through Porous

Media. Part 1: The Dry-Out Effect. *Energy Fuels* **2013**, *27* (5), 2363–2375. DOI: 10.1021/ef302036s.
(18) Moradi-Araghi, A.; Johnston, E. L.; Zornes, D. R.; Harpole, K. J. Laboratory Evaluation of Surfactants for CO2-Foam Applications at the South Cowden Unit **1997**, SPE 37218.
(19) Rossen, W. R.; Boeije C. S. Fitting Foam Simulation Model Parameters for SAG Foam Applications. *SPE* **2013**.
(20) Zhou, Z. H.; Rossen, W. R. Applying Fractional-Flow Theory to Foam Processes at the "Limiting Capillary Pressure". *SPE Advanced Technology Series* **1995**, *3* (1).
(21) Dholkawala, Z. F.; Sarma, H. K.; Kam, S. I. Application of fractional flow theory to foams in porous media. *Journal of Petroleum Science and Engineering* **2007**, *57* (1-2), 152–165.
(22) A. H. Falls, G. J. Hirasaki, T. W. Patzek, D. A. Gauglitz, D. D. Miller, T. Ratulowski. Development of a Mechanistic Foam Simulator: The Population Balance and Generation by Snap-Off. *SPE Reservoir Engineering* **1988**.
(23) Kovscek, A. R.; Patzek T. W.; Radke, C. J. Mechanistic Prediction of Foam Displacement in Multidimensions: A Population Balance Approach. *SPE/DOE* **1994**, *27789*.
(24) Rossen, W. R. Numerical Challenges in Foam Simulation: A Review. *SPE* **2013**.
(25) Arts, R. J.; Vandeweijer, V. P.; Hofstee, C.; Pluymaekers, M.; Loeve, D.; Kopp, A.; Plug, W. J. The feasibility of CO2 storage in the depleted P18-4 gas field offshore the Netherlands (the ROAD project). *International Journal of Greenhouse Gas Control* **2012**, *11*, S10-S20. DOI: 10.1016/j.ijggc.2012.09.010.
(26) Dake, L. P. Darcy's Law and Applications. *Fundamentals of Reservoir Engineering*; pp 103–131.
(27) Review of Leakage from Geological Storage Reservoirs. *International Energy Agency Greenhouse Gas R&D Programme* **2003**, 21.
(28) Spirov P.; Rudyk N. S.; Khan A. A. Foam Assisted WAG, Snorre Revisit with New Foam Screening Model. *SPE* **2012**.
(29) Tsau, J.-S.; Heller, J. Evaluation of Surfactants for CO2-Foam Mobility Control. *SPE PBOGRC* **1992,** SPE-24013-MS.
(30) Manlowe, D. J.; Radke, C. J. A Pore-Level Investigation of Foam/Oil Interactions in Porous Media. *SPE Reservoir Engineering* **1990**, *5* (04).
(31) Chauveteau, G.; Zaitoun, A. Basic rheological behavior of xanthan polysaccharide solutions in porous media: effects of pore size and polymer concentration **1981**, *Developments in Petroleum Science 13, Enhanced Oil Recovery: Proceedings of the Third European Symposium on Enhanced Oil Recovery*, 197–212.
(32) L. Pedroni. *Private communications*.
(33) Pizzocolo, F.; Hewson, C. W.; ter Heege, J. H. Polymer-Gel Remediation of CO2 Migration through Faults and Caprock: Numerical Simulations Addressing Feasibility of Novel Approaches. *ARMA proceedings* **2016**, *50th U.S. Rock Mechanics/Geomechanics Symposium, 26-29 June, Houston, Texas*.
(34) Bernard G.G.; Holm L. W. Model Study of Foam as a Sealant for Leaks in Gas Storage Reservoirs. *SPE 2353*.
(35) Wassmuth; L. H. Hodgins; L. L. Schramm; S. M. Kutay. Screening and Coreflood Testing of Gel Foams To Control Excessive Gas Production In Oil Wells. *SPE 59283*.